

## Article

# Experimental Study of the Rheology of Grease by the Example of CIATIM-221 and Identification of Its Behavior Model

Yuriy O. Nosov  and Anna A. Kamenskikh \* Department of Computational Mathematics, Mechanics and Biomechanics, Perm National Research Polytechnic University, 614990 Perm, Russia; [ura.4132@yandex.ru](mailto:ura.4132@yandex.ru)\* Correspondence: [anna\\_kamenskikh@mail.ru](mailto:anna_kamenskikh@mail.ru); Tel.: +7-(342)-2-39-15-64

**Abstract:** The study of the rheological properties of a lubricant allows for the assessment of the structure's durability in which they are used. Computer engineering enables the prediction of the structure performance using refined mathematical models of its materials. This paper presents an experimental investigation of the rheological behavior of a lubricant that is actively used in bridge structures. The paper proposed a methodology for determining the rheological characteristics of the lubricant using a rotational viscometer. Additionally, the article performed the task of identifying the mathematical model of the lubricant behavior based on the Maxwell body, using two approaches: the Anand model and the Prony series. The proposed models allow for numerical modeling of the structure's performance throughout their lifecycle within the scope of computer engineering.

**Keywords:** lubricant; viscoelastic; Prony series; Anand's model; viscosity; elastic; oscillation experiment; experimental data; numerical data

## 1. Introduction

### 1.1. Research Objectives

Research objective: conducting full-scale experiments and identifying a mathematical model of the viscoelastic lubricant behavior over a wide temperature range.

Research and development objectives:

1. Conducting a series of full-scale experiments to determine the viscoelastic lubricants properties over a wide range of temperatures;
2. Identifying a mathematical model of the viscoelastic lubricant behavior in the form of the Maxwell body based on two viscoelasticity models: the Prony series and the Anand's model;
3. Creating a unified numerical procedure to determine approaches to the parameters from item two based on the application of the multi-parameter Nelder–Mead optimization.

### 1.2. Problem Context and Description

Various lubricants are widely used in friction nodes [1–6]. Such structures operate within the framework of solid mechanics and contact mechanics. In operation, lubrication helps to reduce friction between contact surfaces [7,8], reduce the effect of surface roughness [9,10], control the temperature [11,12], etc. At the same time, many authors note the nonlinear lubricant behavior during operation [10,13–15]. Numerical models require a qualitative description of the material behavior as close to real constructions as possible. Lubricants are no exception; thus, it is necessary for the detailed study of the application of a mathematical model to describe the lubricants behavior.

At present, lubricants are divided into four groups: liquid, plastic, solid, and gaseous. Depending on their aggregate state, lubricants may be used in various areas of human activity: machine building [16,17], bridge building [18], hydraulic systems [19], etc. Lubricants



**Citation:** Nosov, Y.O.; Kamenskikh, A.A. Experimental Study of the Rheology of Grease by the Example of CIATIM-221 and Identification of Its Behavior Model. *Lubricants* **2023**, *11*, 295. <https://doi.org/10.3390/lubricants11070295>

Received: 16 May 2023

Revised: 4 July 2023

Accepted: 13 July 2023

Published: 15 July 2023



**Copyright:** © 2023 by the authors. Licensee MDPI, Basel, Switzerland. This article is an open access article distributed under the terms and conditions of the Creative Commons Attribution (CC BY) license (<https://creativecommons.org/licenses/by/4.0/>).

work under different conditions in structures. Lubricant works in a state of constrained compression [18] and within the framework of thermomechanics and thermal application in bridge bearing structures. It increases the structure durability and improves the heat transfer efficiency of the condenser and evaporator [19]. Lubricants are an integral part of the actual tribology problem [20]. In this case, several works [21–23] point out the importance of conducting full-scale and numerical experiments to determine the properties and perform mathematical modeling of their behavior.

Computer engineering enables a numerical analysis of the structure to be conducted, assessing the possibility of using different materials in the structure, analyzing the influence of changes in geometry, and so on. Computer engineering allows for the rationalization of the structure and its elements relatively quickly. It is necessary to use material behavior models that are close to reality to obtain high-quality modeling results. Many authors emphasize the importance of constructing mathematical models of material behavior [24–28]. This allows for an approximation of the model to the actual structure.

One of the actual problems is the study of the dynamic characteristics of the lubricant behavior [21–23,29–31], including the viscoelasticity, viscoplasticity, etc. Many studies [32,33] describe lubrication by Maxwell-type equations. Maxwell's body is a viscoelastic fluid that can flow (relax) under any load. It is characterized by irreversible deformations [30]. The Prony series and Anand's model are the most common models for describing the Maxwell's body. The Prony series is widely used to describe the viscoelastic behavior of various materials [34–36]. This approach is applied to polymeric [37,38] and metallic materials [39]. The description of viscoelasticity by Anand's model enables the evaluation of the material plastic deformation. Initially, Anand's model was aimed at describing the behavior of metal melts [40,41]. Later, it was widely used to describe polymers, pure and alloyed glasses, composites, etc. [42,43]. An incomplete set of model parameters is often used when describing non-metallic materials. This is due to the peculiarities of the material behavior being described. At present, there are attempts to describe lubricant behavior based on the mathematics of Anand's model [44].

To describe the mathematics associated with the operation of lubricants, it is necessary to use methods of computer engineering and numerical algorithms. Thus, it is possible to automate the search for the coefficients of the defining relationships and conduct verification of the obtained data based on numerical and full-scale experiments. Such approaches are widespread and have proven their effectiveness in determining the materials characteristics [45].

The main directions of lubricant research can be distinguished as follows:

1. Study of tribological, electromechanical, and thermal characteristics of lubricants, including those with various additives and solutions;
2. Experimental research on a wide range of temperatures to identify dynamic and static characteristics;
3. Identification of mathematical models of material behavior and their implementation in numerical analogues of friction nodes.

Currently, there are various methods for researching the rheological characteristics of lubricants, including capillary viscometers, penetrometers, rotational viscometers, DWS technology, etc. The principle of capillary viscometers is based on determining the flow rate of the fluid under the influence of a pressure difference in the capillary [46,47]. Penetrometers determine the resistance of the lubricant by measuring the penetration of indenters with different geometrical, physical, and mechanical characteristics into the lubricant [48]. Rotational rheometers are characterized by coaxial cylindrical viscometers, which consist of two cylinders of the same size, one of which is fixed, and the other rotates around its axis at different frequencies [47–51]. DWS technology [52] is significantly different from other methods, requiring a minimal amount of sample. Spectroscopy allows for non-contact investigation of the sample, which eliminates the possibility of sample destruction. This type of technology allows for the evaluation of the rheological material properties over a wider range of temperatures and frequencies compared to analogs. The lubricant examined

in this study is used in sliding bridge bearings. These structures work within a narrow temperature range of  $-60$  to  $60$  °C and at higher shear rates. In the first approximation, it was decided to investigate the material on the Discovery HR2 rotational viscometer. DWS technology will be used for further research on the behavior of the lubricant.

The current research is aimed at obtaining an experimental basis for the deformation behavior of lubricants with refinement of the experimental research methodology. The second direction of the research is creating effective numerical algorithms to describe pasty lubricants using well-known models widely used in applied engineering analysis packages: ANSYS Mechanical APDL (ANSYS Inc., Canonsburg, PA, USA); ABAQUS (ABAQUS Inc., Velizy-Villacoublay, France), etc. Lubricants are used in the steel–polymer contact material pair structure, which can operate in a wide temperature range to ensure the durability. They include CIATIM-221, CIATIM-221F, TOMFLON SK 170 FH, TOMFLON SBS 240 FM, etc. CIATIM-221 and CIATIM-221F are produced all over the world. This paper presents the performance of full-scale experiments to determine the rheological properties of the lubricant CIATIM-221 (Center-Oil LLC, Polevskoy, Russia) over a wide temperature range. The identification of a mathematical lubricant model is required for further investigation of the design performance through numerical experiments.

## 2. Materials and Methods

### 2.1. Experimental Research

The lubricant CIATIM-221 was chosen as the research object. It is a frost- and heat-resistant lubricant, which allows its use in both hot and northern climatic zones.

Experimental studies are conducted at the premises of the PNIPU plastics laboratory. Thermophysical, rheological, and thermomechanical characteristics of the materials and products are tested in the laboratory [53,54]. A Discovery Hybrid Rheometer (TA Instruments—Waters LLC, New Castle, DE, USA) (Figure 1a) was used for experimental investigation of the rheological lubricant characteristics. The main characteristics are:

- minimum oscillation torque 2;
- minimum sustained shear torque 10;
- maximum torque 200;
- torque resolution 0.1;
- minimum frequency;
- maximum frequency 100;
- minimum angular frequency 0;
- maximum angular frequency 300;
- displacement resolution 10, etc.

An electrically heated plane is used for the active heating and cooling of the study samples. This design allows the specimens to be heated to  $400$  °C and cooled to  $-70$  °C using liquid nitrogen (Figure 1b). The design allows for a uniform temperature distribution throughout the sample. As part of the operation, the temperature tolerance limit is  $\pm 1$  °C.

To determine the true stresses and strains during the experiment, it is necessary to consider the measuring system. As part of the work, a comparison of two variants of measuring systems was performed: plane–plane and cone–plane. The basic relationships for determining the stress (1) and strain (2) are as follows:

$$\sigma = K_{\sigma} \cdot M, \quad (1)$$

$$\gamma = K_{\gamma} \cdot \varphi, \quad (2)$$

where  $M$ —rheometer torque;  $\varphi$ —offset angle;  $K_{\sigma}$  and  $K_{\gamma}$ —stress and strain constants, respectively, which depend on the geometry of the mating surfaces. According to [55], dynamic tests are run in the framework of linear viscoelasticity. This allows the specimens to be examined without destroying the structure. To determine the viscoelastic characteristics of the material, we will use a technique that consists of 4 stages.

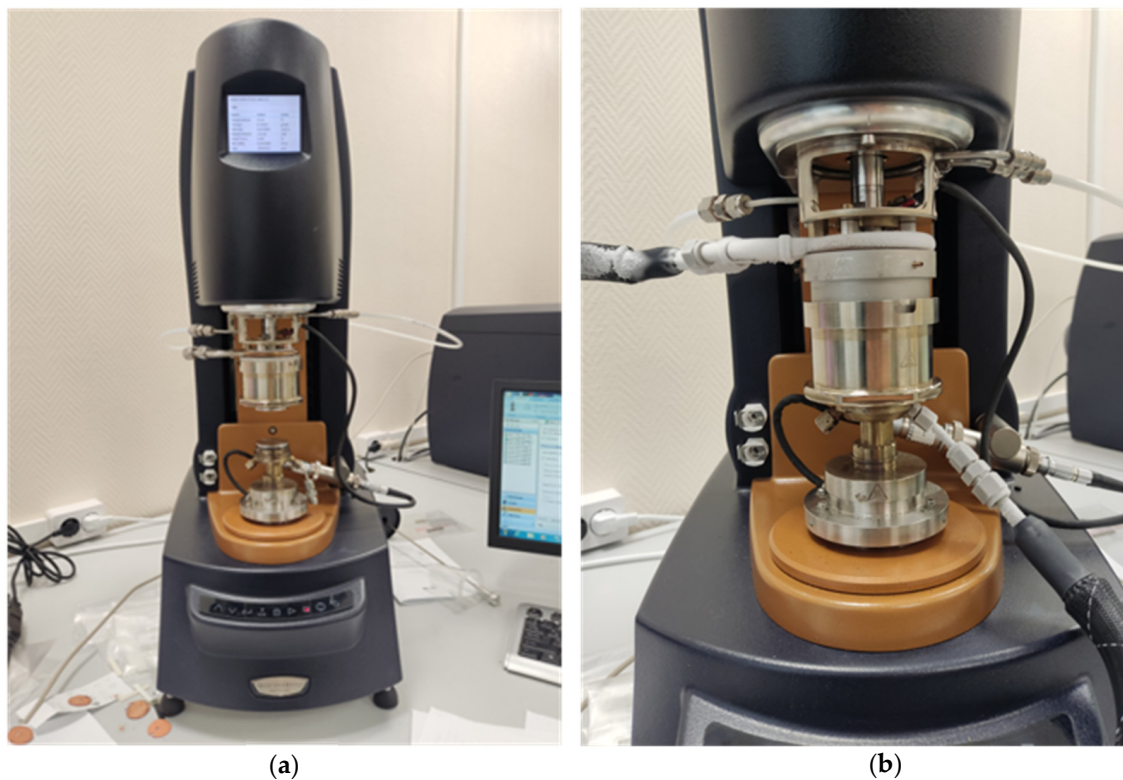


**Figure 1.** Experimental study on the Discovery HR2 rheometer. (a) General view of the setup; (b) application of liquid nitrogen.

In the first stage of the studies, it is necessary to determine the shear value of the sample [56]. To determine the linear viscoelasticity domain, a strain sweep experiment is conducted in which the value of the complex shear modulus  $G^* = \text{const}$  is monitored.

The second stage of the study is the selection of the measuring system for dynamic tests. Two options can be considered with the presented equipment: cone–plane [57] and plane–plane [58]. The main advantage of the cone–plane measuring system is the uniform shear rate distribution. However, due to the small gap size (50–100 times smaller than for the second variant), there are errors in the investigation of temperature dependence.

The third stage of the study involves a series of experiments to determine the dependence of the material properties on temperature [59]. The sample is dynamically deformed at a small displacement angle, which is determined at stage 1 of the study, with a constant shear rate and cooling/heating of the sample at a constant rate.

The final stage of the study consists of determining the dependence of the material stresses on the shear rate [60]. Similar to stage 3, the material is deformed, the temperature remains constant, and the shear rate changes.

## 2.2. Identification of a Mathematical Model of Lubricant Behavior

In [32,33], the lubricant is described as a Maxwell body. It is a sequential connection of an elastic spring (3) and a viscous element (4):

$$\tau_e = G\gamma_e, \quad (3)$$

$$\tau_v = \eta\dot{\gamma}_v, \quad (4)$$

where  $G$ —shear modulus;  $\eta$ —dynamic viscosity. Thus, the elastic and viscous element tangential stresses are equal to each other (5), and the shear strain is the sum of the elastic and viscous parts (6) in the case of a series connection:

$$\tau = \tau_e = \tau_v, \quad (5)$$

$$\gamma = \gamma_e + \gamma_v. \quad (6)$$

Total shear strain as a function of time:

$$\gamma = \tau/G + 1/\eta \left( \int_0^t \tau(q) dq \right). \quad (7)$$

Further research is based on Equations (3)–(7).

The search for unknown parameters of the presented models is performed using the multi-parameter Nelder–Mead optimization algorithm with experimental data. The problem of minimization of the functional is as follows:

$$F = |(\tau_{\text{exp}} - \tau_{\text{num}}(\bar{x})) / \tau_{\text{exp}}| \times 100\% \rightarrow \min, \quad (8)$$

where  $\bar{x}$ —vector of unknowns.  $\bar{x}$  has a different number of optimization parameters for different viscoelastic models. The search continues until the functional is less than 5%.

### 2.2.1. Prony Series

The Prony series in conjunction with the Williams–Landela–Ferry (*WLF*) model allow the behavior of a material to be described over a wide temperature range. The stress–strain relationship has the form:

$$\tau(t) = \int_0^t 2 \left[ G_\infty + G_0 \sum_{i=1}^k \alpha_i \exp(-(t-q)/\beta'_i) \right] d\gamma(q), \quad (9)$$

where  $G_0$ —shear modulus at  $t = 0$ ;  $k$ —the number of Prony series variables;  $q$ —relaxation time;  $\alpha_i$ —shear modulus coefficients. The experimental data are given in the form of a shear modulus distribution as a function of temperature. The temperature–time analogy *WLF* (10) is used to identify the model:

$$\beta'_i = \beta_i / A_{WLF}(T), \quad (10)$$

where  $A_{WLF}(T)$ —the shift function used in the *WLF*, which is of the form:

$$A_{WLF}(T) = (C_1(T - T_r)) / (C_2 + (T - T_r)), \quad (11)$$

where  $T$ —current temperature;  $T_r$ —constant baseline temperature;  $C_1$ ,  $C_2$ —empirical material constants.

Based on Equations (9)–(11), the unknowns vector  $\bar{x} = \{\beta_i, \alpha_i, T_r, C_1, C_2\}$  is constructed, which is retrieved by minimizing the functional (8).

### 2.2.2. Anand's Model

Anand's model allows for the description of not only the viscoelastic but also the plastic behavior of the materials. It includes the viscous shear rate:

$$\dot{\gamma}_v = A e^{-U/RT} [\sinh(\xi\tau/S)]^{1/m}, \quad (12)$$

and the evolutionary equation:

$$\dot{S} = \{h_0(|B|^a B / |B|\} \dot{\gamma}_v, \quad (13)$$

where  $B = 1 - S/S^*$ ;  $S^* = S_1 [\dot{\gamma}_v e^{U/RT}/A]^n$ ;  $S$ —strain resistance;  $S^*$ —the saturation value of the hardening function;  $h_0$ —material curing constant;  $R$ —universal constant gas;  $U$ —activation energy;  $T$ —absolute temperature;  $n$ —sample saturation as a function of shear rate. Based on Equations (12) and (13), the unknowns vector  $\mathbf{x} = \{S_0, A, U/R, \xi, m, h_0, S_1, n, a\}$  is constructed.

To describe the Maxwell body, transform Equation (4) to the form (12):

$$\dot{\gamma}_v = \tau/\eta = A e^{-U/RT} [\sinh(\xi\tau/S)]^{1/m}, \quad (14)$$

by adopting a number of simplifications ( $m = 1$ ;  $\xi \ll 1$ ;  $S = 1$ ), Equation (14) takes the form:

$$\dot{\gamma}_v = \tau/\eta = A \xi e^{-U/RT} \tau, \quad (15)$$

where a number of empirical constants and dynamic viscosity  $\eta = e^{U/RT}/(A\xi)$  are related, which can be determined from the experimental data. With  $S = 1$ , Equation (13) is zeroed. Then,  $h_0 = 0$ , and the vector of the unknowns takes the form  $\mathbf{x} = \{S_0, A, U/R, e^{U/RT}/(A\xi), 1, 0, S_1, n, a\}$ . Transforming  $\mathbf{x}$  by excluding the known constants and relationships, the final vector of unknowns takes the form  $\mathbf{x} = \{S_0, A, U/R, S_1, n, a\}$ .

### 2.3. Mathematical Model Identification Procedure

The identification procedure is built on the synergy of ANSYS and Python. A pure shear numerical experiment is simulated in ANSYS Mechanical APDL (Figure 2).

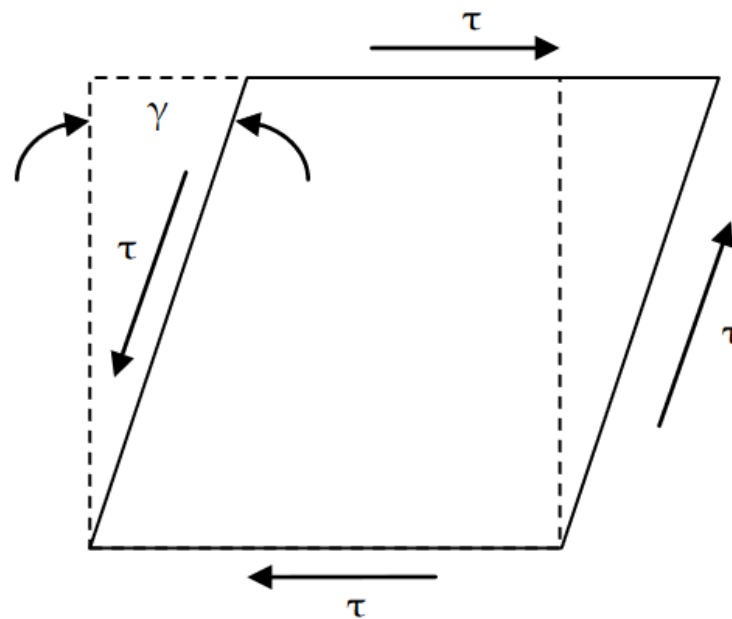


**Figure 2.** Numerical experiment for pure shear.

The shear value of the sample corresponds to the experimental data of 0.1%. This repeats the cyclic shear strain of the sample over a wide temperature range from 80 to  $-40$  °C a rate of 2 °C per minute. A simplified scheme of the mathematical model identification procedure is shown in Figure 3.



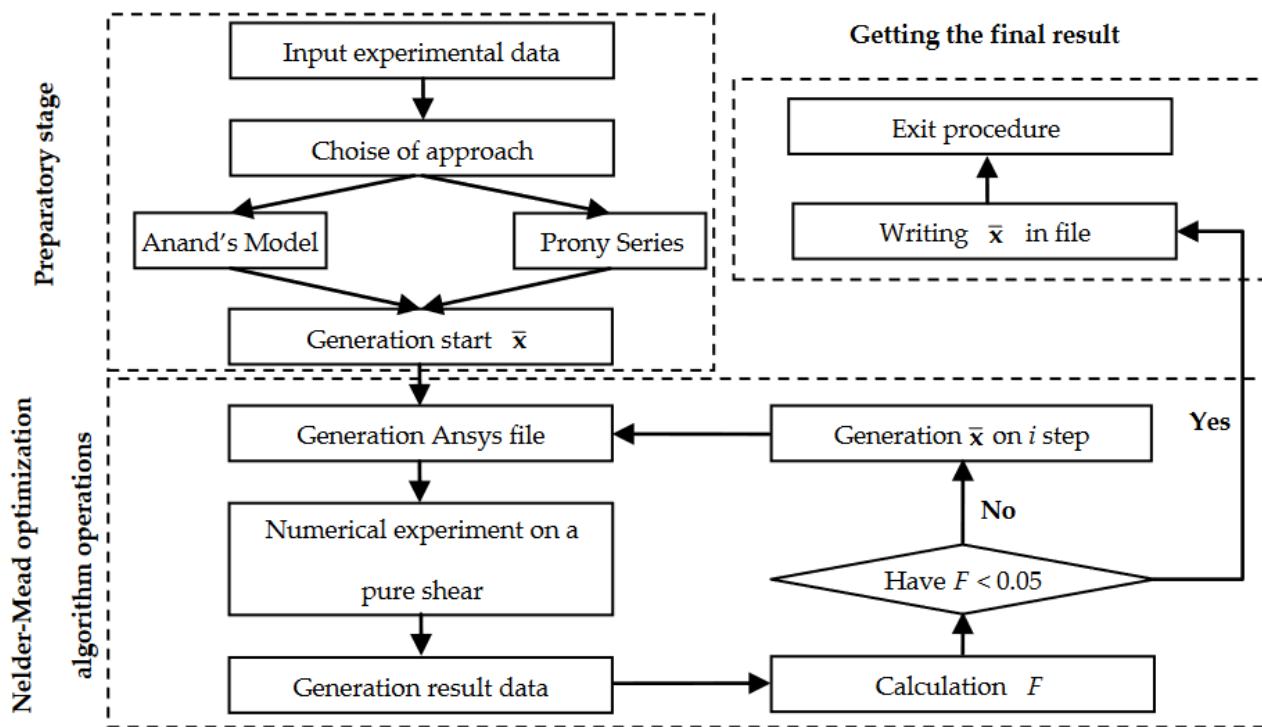


Figure 3. Simplified scheme of the mathematical model identification procedure.

The numerical procedure consists of 3 main parts:

- Preliminary step. It consists in the form of experimental data into the procedure, the choice of a mathematical model, and the setting of initial values of the unknowns vector  $\bar{x}$ ;
- Nelder–Mead multi-parameter optimization operations. An ANSYS file is generated with a sequence of commands to build the numerical model. The pure shift problem is solved with the generation of a results file. The function  $F$  is calculated and comparing to the required error. If the condition is not met, a new vector of unknowns is generated. Then, the optimization procedure is repeated;
- Obtaining a result file. If the error condition is met, the final value of the unknowns vector  $\bar{x}$  is written down and the procedure is exited.

### 3. Results

#### 3.1. Results of Full-Scale Experiments

Friction nodes often operate in aggressive environments, under increased loads, in temperature zones with elevated/reduced temperatures and frequent temperature fluctuations. CIATIM-221 is often used in the sliding bearings of bridges [61–63]. These structures operate in the temperature range  $-60$  to  $60$  °C. Research has been performed on the temperature range of  $-40$  to  $80$  °C. This range includes most of the operating ranges of plain bearings.

The shear strain limit of the lubricant has to be estimated in the first phase of the study. This is necessary to determine the linear viscoelasticity interval (Figure 4). According to [56], the limit of the linear viscoelasticity interval decreases as the temperature increases. Consequently, the study will be conducted at elevated temperatures close to the maximum values:  $50$  °C and  $80$  °C. The study was performed using two measuring systems: plane–plane and cone–plane.

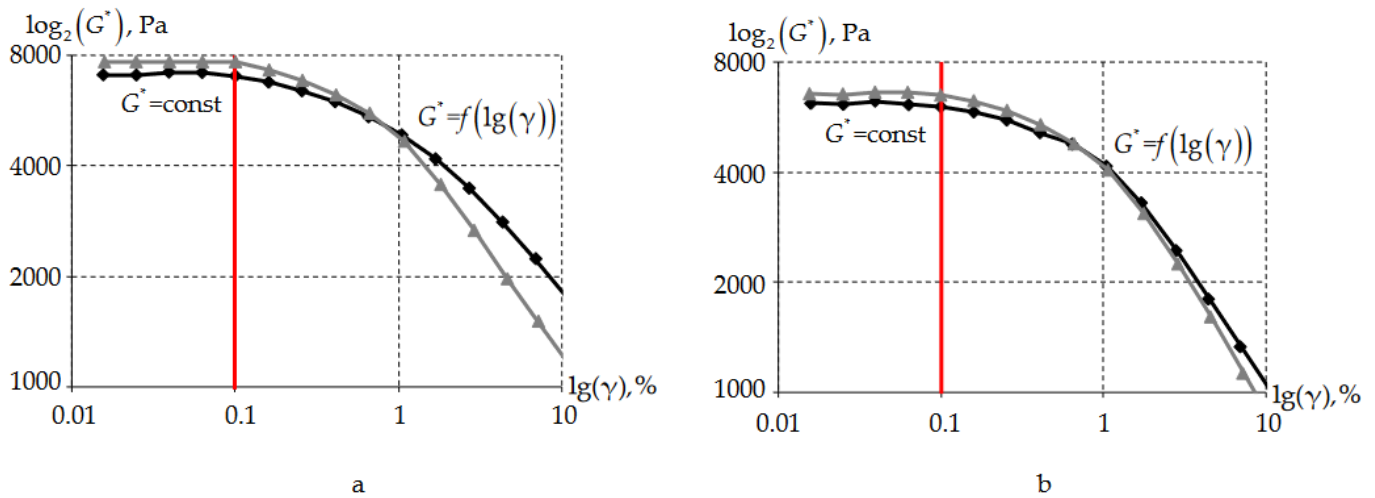


**Figure 4.** Linear viscoelasticity limit analysis: (a) 50 °C, (b) 80 °C; measuring systems: black line—plane–plane, gray line—cone–plane.

The distribution of the complex modulus has a nonlinear characteristic after the shear strain of the sample reaches more than 0.1%. Consequently, in the next stages of the viscoelasticity study, the lubricant will be subjected to a shear strain value of 0.1%. In addition, at the linear viscoelasticity interval, the cone–plane measuring system has values higher by an average of 3% than the plane–plane measuring system.

Next, tangential stresses are investigated as a function of shear rate. Experiments are conducted at temperatures of 50 and 80 °C. Within the study, a shear rate of 100 Hz is the maximum possible value. The minimum value of the shear rate was chosen out of consideration of the time cost of the experiment. To obtain the value, it is necessary to perform three to five stress measurements [32,33] at each value of the shear rate (Figure 5).

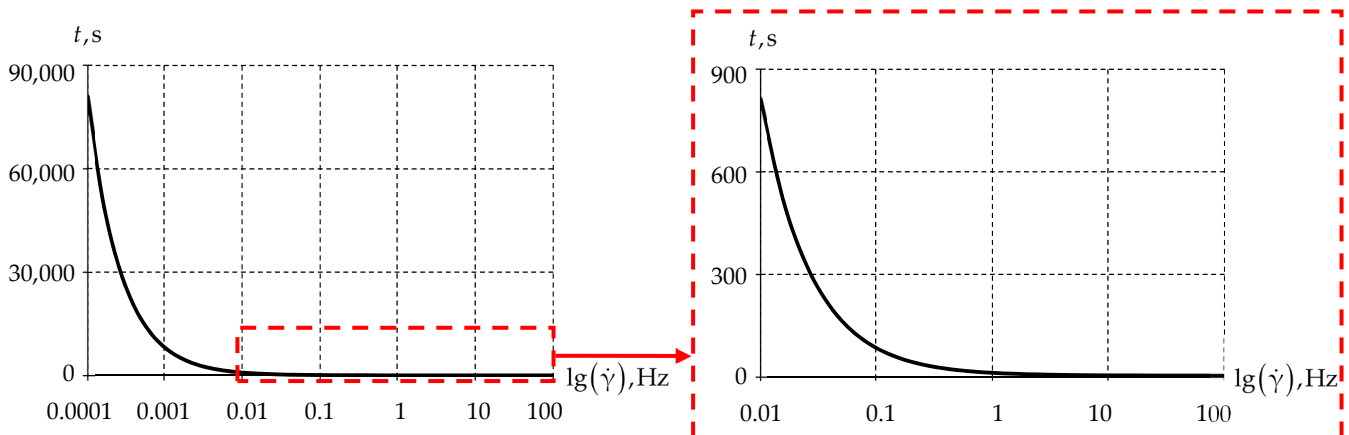


**Figure 5.** Dependence of the experiment time on the choice of the minimum shear rate.

An increase in the experiment time is observed with a decrease in the minimum value of the shear rate. In this case, the experiment time is presented without taking into account the inertial loads. The elimination of the inertia leads to an increase in the experiment time by an average of 20–30%. It was decided to use a range of shear rates (0.01 Hz to 100 Hz) to minimize the time of the experiment.

In the second stage of the study, it is necessary to determine the measuring system. For this purpose, we will conduct experiments on the dependence of tangential stresses on the shear rate at temperatures of 50 °C and 80 °C (Figure 6).



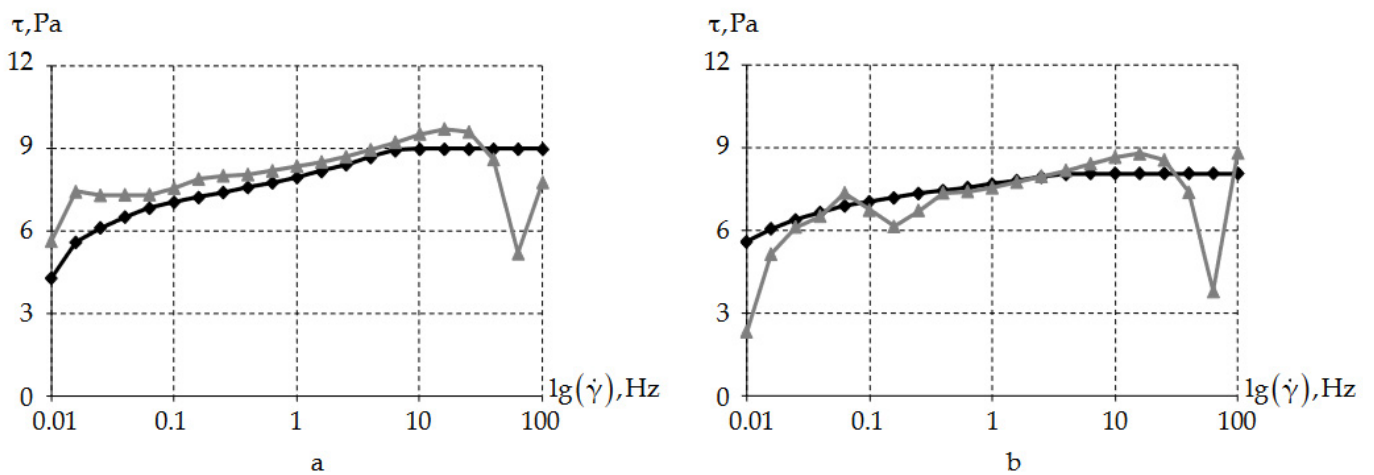


**Figure 6.** Comparison of measuring systems: (a) 50 °C, (b) 80 °C; measuring systems: black line—plane–plane, gray line—cone–plane.

The value of the tangential stresses when using the cone–plane measuring system is non-uniform. With the plane–plane system, the dependence  $\tau(\lg(\dot{\gamma}))$  is uniform. It becomes constant at a certain shear rate. The cone–plane measuring system introduces a significant error at temperatures other than room temperature.

The third stage of the study consists of conducting experiments to determine the dependence of the material properties on temperature. For this purpose, a sample shear strain value of 0.1% and an average shear rate of 1 Hz are chosen based on stages 1 and 2. The sample is cooled from 80 °C to −40 °C a rate of 2 °C per minute (Figure 7).

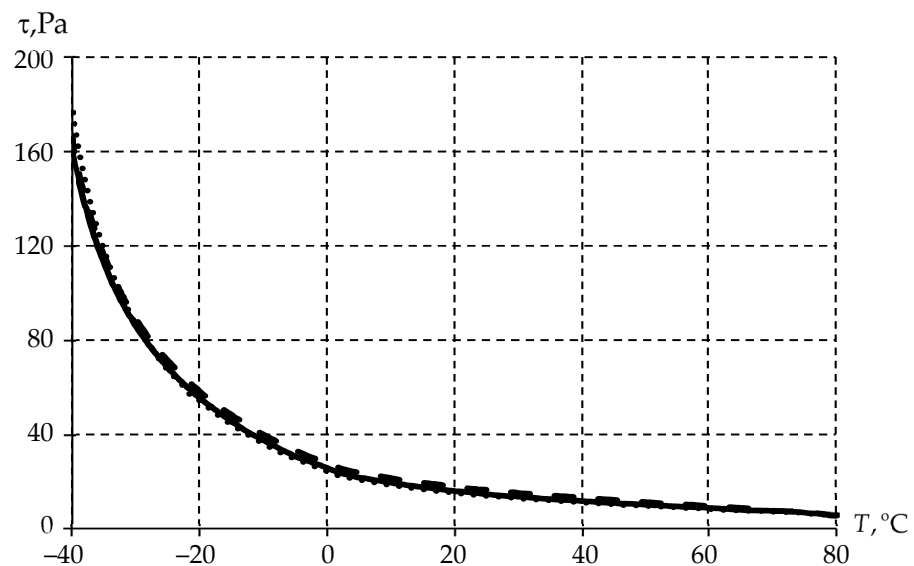


**Figure 7.** Dependence of tangential stress on temperature in a series of experiments: solid line—experiment 1; dashed line—experiment 2; dots—experiment 3.

The distribution of tangential stresses as a function of temperature is exponential. A significant increase in tangential stresses occurs at temperatures less than 0 °C. The difference does not exceed 5% in the experimental data.

In addition, temperature dependence was obtained for the following lubricant characteristics: complex shear modulus, accumulation modulus, and loss modulus. These characteristics serve us to assess its aggregate state (Figure 8).

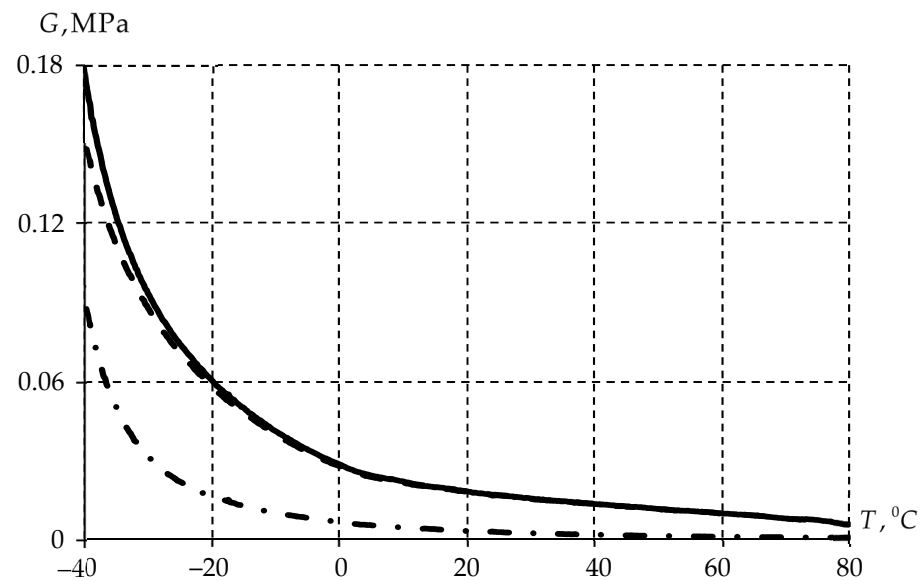


**Figure 8.** Dependence of physical and mechanical characteristics of a lubricant on temperature: solid line—complex shear modulus; dashed line—accumulation modulus; dash-dot line—loss modulus.

The distributions of the complex modulus, accumulation modulus, and loss modulus have similar characteristics. The distribution is exponential with a decreasing sample temperature. Over the entire temperature interval, the accumulation modulus is higher than the loss modulus. According to [55,56], this behavior indicates a constant aggregate state of the material as an elastic or gel-like body.

As part of the lubricant research methodology, the last step is to analyze the behavior of the sample when the shear rate changes. The experiment is conducted at a number of temperatures:  $-40\text{ }^{\circ}\text{C}$ ,  $-20\text{ }^{\circ}\text{C}$ ,  $0\text{ }^{\circ}\text{C}$ ,  $20\text{ }^{\circ}\text{C}$ ,  $50\text{ }^{\circ}\text{C}$ , and  $80\text{ }^{\circ}\text{C}$  (Figure 9).

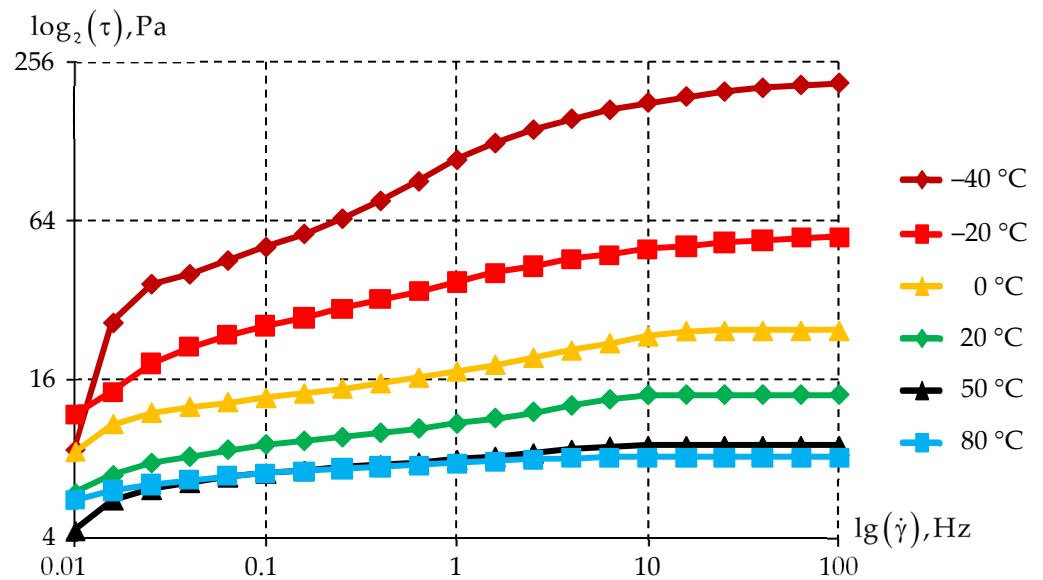


**Figure 9.** Tangential stress distribution as a function of shear rate.

The behavior of tangential stresses as a function of shear rate for non-negative temperatures minimally differs. The values increase by gradually reaching a constant value when a certain shear rate is obtained. The boundary of constant tangential stress increases as the temperature decreases. In the case of negative temperatures, there is no such interval.

### 3.2. Identification of a Mathematical Model of the Lubricant as a Function of Temperature

A pure shear numerical experiment is simulated as part of the identification of the mathematical model of the lubricant. The numerical experiment corresponds to the laboratory experiment: shear strain value at 0.1% with a shear rate of 1 Hz and a temperature rate of 2 °C per minute.

The experimental data were approximated over the range of  $-40$  to  $80$  °C, with a rate of 2 °C, to compare the values of tangential stress. Tangential stress values corresponding to the experimental data will be collected every 60 s (Figure 10), in the process of solving the dynamic problem in a numerical experiment.

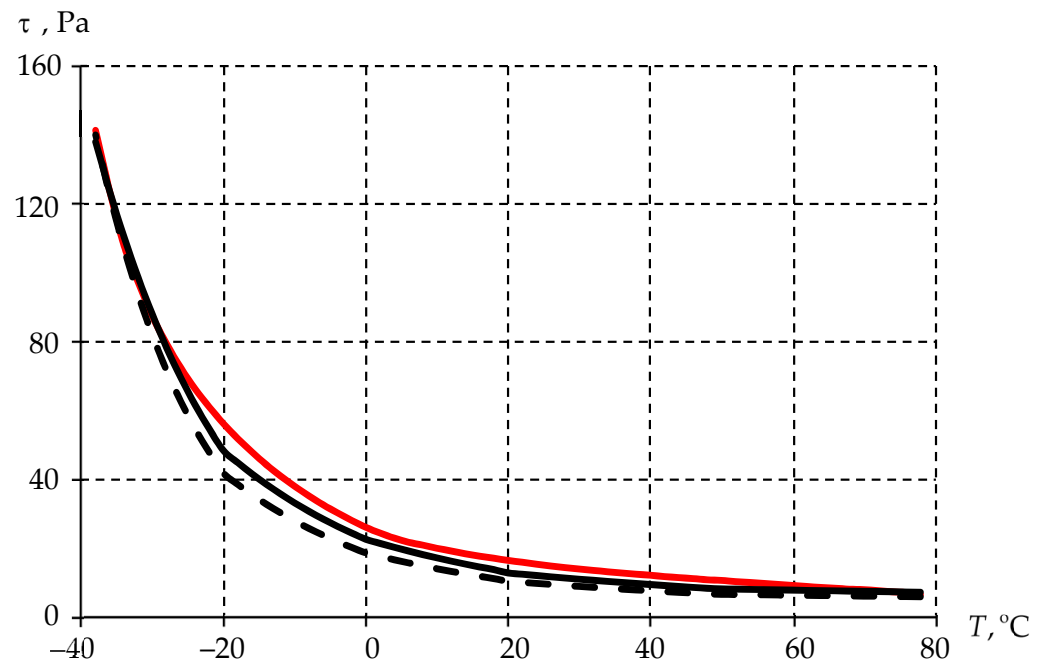


**Figure 10.** Tangential stress distribution as a function of temperature: red line—approximation of experimental data; solid black line—Anand’s model; dashed black line—Prony series.

The experimental dependence  $\tau(T)$  is obtained on the basis of statistical data processing. An approximation of the function of voltage dependence on temperature was carried out. Further studies are based on this curve. The scatter of experimental results does not exceed 5%. The identification procedure with the use of two mathematical approaches allows us to obtain  $\tau(T)$  at a sufficiently good level.

The relaxation times  $\beta_i$  of the Prony series include 21 coefficients in the range of  $10^{-10}$  to  $10^{10}$ . The initial distribution of the weight coefficients,  $\alpha_i$ , was set as constant, equal to 0.01. In the course of the algorithm’s work, the value of the weight coefficients changed significantly (Figure 11).

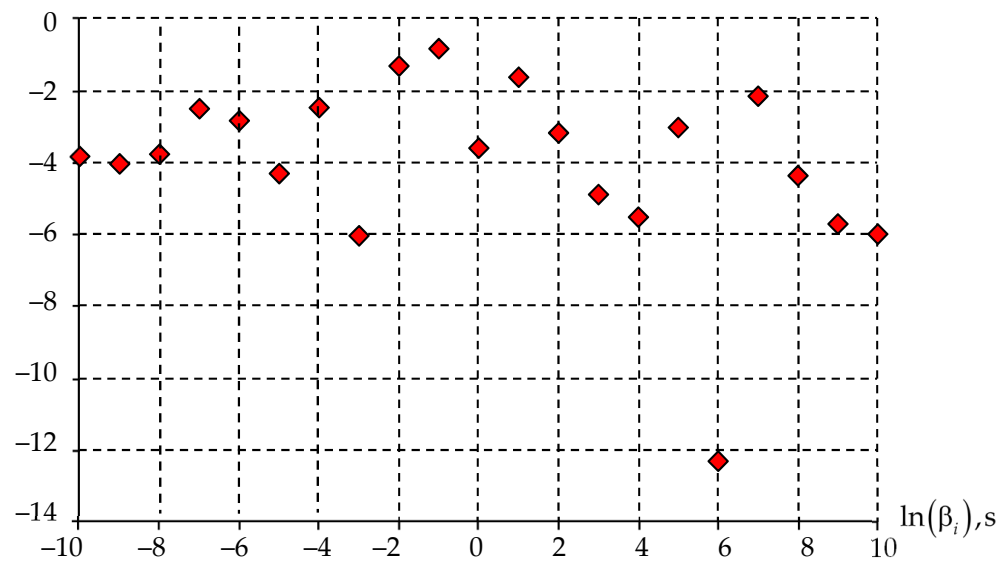


**Figure 11.** Final distribution of the Prony model coefficients for CIATIM-221.

It can be seen that the weight coefficient at a relaxation time of 10 s has a significant effect. In addition, the values of the coefficients of Equation (11) have the form:  $T_r = 12.1513$  K,  $C_1 = 4.1469$ ,  $C_2 = 20.5555$ .

The numerical procedure for identifying Anand's model converges much faster. This is due to a smaller set of material constants. Table 1 shows the initial and final values of the coefficients of Anand's model.

**Table 1.** Value of Anand's model coefficients for CIATIM-221.

Values	$S_0$ , MPa	$A$ , 1/s	$U/R$ , K	$S_1$ , MPa	$n$	$a$
Initial	1	$10^{10}$	1000	1	1	1
Final	15.6218	$3.518 \times 10^9$	985.0634	$7.023 \times 10^{-7}$	$4.498 \times 10^{-4}$	2.8112

The initial shear strain resistance value,  $S_0$ , is related to the significant viscosity of the lubricant. The shear strain resistance saturation coefficient,  $S_1$ , decreases with exposure time. The decrease,  $n$ , can be attributed to the shear yield characteristic of the lubricant.

### 3.3. Dependence of Rheological Properties of the Lubricant on the Shear Rate

A characteristic feature of pasty lubricants is the predominance of the viscous component at low shear rates and the elastic component at higher shear rates. It is necessary to investigate the lubricant's dependence on the shear rate. Figure 12 shows the dependence  $\tau(\lg(\dot{\gamma}))$  at different temperatures.

The nature of the tangential stress distribution as a function of shear rate at different temperatures has minor differences; there is a coincidence in the values at shear rates greater than 10 Hz but a significant error at lower shear rates. The Prony series description of grease has a higher error than Anand's model. This is related to the fact that Anand's model accumulates plastic deformation. An extension of the mathematical description of the defining relationships is required in other viscoelastic models for pasty greases.

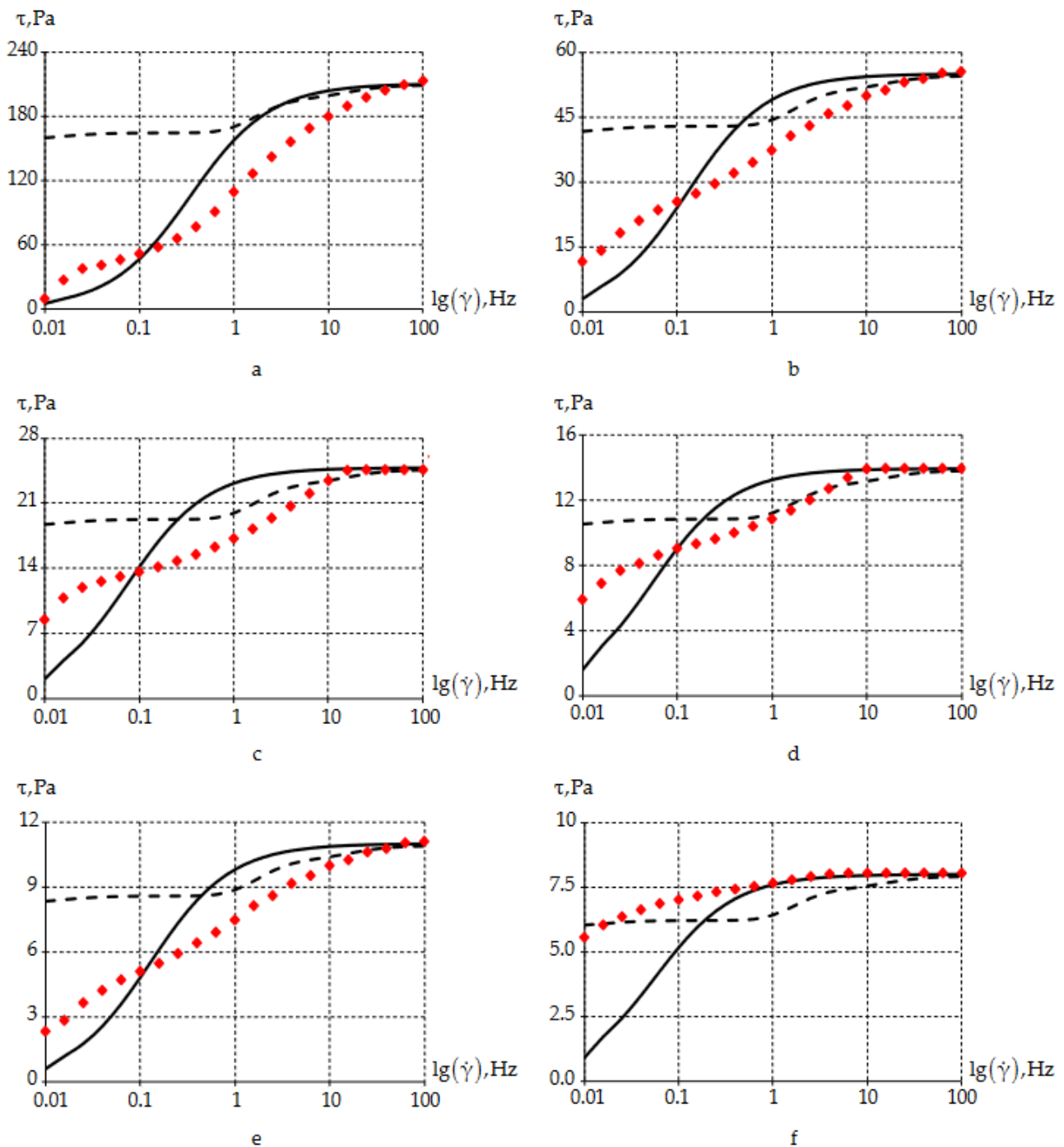


**Figure 12.** Tangential stress distribution as a function of shear rate over a wide range of temperatures: (a)  $-40\text{ }^{\circ}\text{C}$ , (b)  $-20\text{ }^{\circ}\text{C}$ , (c)  $0\text{ }^{\circ}\text{C}$ , (d)  $20\text{ }^{\circ}\text{C}$ , (e)  $50\text{ }^{\circ}\text{C}$ , and (f)  $80\text{ }^{\circ}\text{C}$ ; red markers—experimental data; solid black line—Anand’s model; dashed black line—Prony series.

## 4. Discussion

### 4.1. Limitation Statement

The presented study has several limitations:

- The full-scale experiment is conducted in a small range of shear rates, from 0.01 to 100 Hz, which does not give a complete picture of the viscous and elastic components at small and large share rates, respectively;
- The behavior of the lubricant was investigated using the Discovery HR2 rotational viscometer with a limited range of temperatures and share rates;

- The lubricant is capable of operating in the temperature range of  $-60$  to  $+150$  °C, but the equipment allows evaluation of behavior at temperatures of  $-40$  to  $+80$  °C;
- Lubricant is treated as a Maxwell body, in fact, the object of study has a more complex pattern of behavior;
- Lubricant is considered within the problem of deformable solid mechanics; the problem of fluid and gas mechanics is not set.

In the future, many tasks will be set before the researchers:

- Consideration of other linear viscoelastic models (Kelvin model, Voigt model, etc.);
- Using a temperature–time superposition to be able to describe and analyze decreased and increased shear rates and temperatures;
- Numerical simulation of the structure as a whole with the use of a lubricant, using the example of a spherical sliding bearing of a bridge span;
- The lubricant will be examining using the DWS technology.

#### 4.2. Prediction of Structure Behavior Based on Computer Engineering

Computer engineering allows for predicting the behavior of a structure. To do this, refined mathematical models of the behavior of lubricants should be used [64–66]. Chong et al. conducted research to determine the mathematical model of lubricant behavior, which allows for the accurate prediction of the frictional characteristics of lubrication systems. Mukutadze et al. also conducted research on the mathematical model of liquid lubricant behavior, which allows for predicting the influence of the non-stationary profile on the shear rates, pressure, and friction force of the lubricant. In addition, the authors [66] actively describe the mathematical model of the rheological behavior of lubrication at higher frequencies. Two modes were identified: at high temperature and low pressure, the response is adapted to the Kappo model, and as the viscosity increases, the response changes and is consistent with the theory of Airy. This, in turn, allows for predicting the overall behavior of the structure at higher frequencies of its operation.

This work considers the lubricant CIATIM-221, which is widely used in bridge structures. Identifying the mathematical model allows for predicting the behavior of the structure over a wide range of temperatures. The model can be used under higher frequency loads on the structure. To describe the low-frequency effect on the structure, more complex models, as described above, should be used.

#### 4.3. On the Choice of a Mathematical Model

Many researchers consider a lubricant as a more complex viscoelastic or viscoelastic-plastic body [67,68]. Ivins et al. describe the rheological behavior of a lubricant with the Burger model, which, unlike the Maxwell model, includes two springs and two viscous elements. The description of the rheological behavior of a lubricant by a more complex models leads to refinement of the results on the dependence on shear rates. Kvarda et al. [69] propose to describe the lubricant, at higher shear rates, by Newton's law of viscosity, which is related to the output of a constant stress value, as presented in the experiments in Section 3.1.

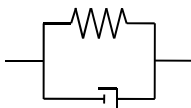
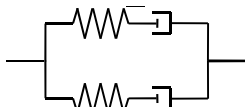
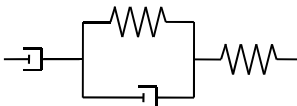
Larson [44] offers several mathematical models to describe a complete model of the rheological behavior of a lubricant: the model of Mujumdar et al. [70], the de Souza Mendes and Thompson model [71], the Radhakrishnan model [72], etc.

The considered mathematical models and relationships for describing the lubricant viscoelastic behavior are presented in Table 2.

The description of pasty greases, such as CIATIM-221, based only on the Maxwell equations for a wide range of temperatures and shear rates is impossible. Selection of a mathematical model is required, which will allow a better description of the complex behavior of greases at a wide range of temperatures and shear rates.



**Table 2.** Mathematical models for describing the lubricant viscoelastic behavior.

Mathematical Model	Scheme of the Model	Equation
Kelvin–Voigt model		$\sigma(t) = E\varepsilon(t) + \eta \frac{d\varepsilon(t)}{dt}$
Burgers Material (Maxwell representation)		$\sigma + \left( \frac{\eta_1}{E_1} + \frac{\eta_2}{E_2} \right) \dot{\sigma} + \frac{\eta_1 \eta_2}{E_1 E_2} \ddot{\sigma} = (\eta_1 + \eta_2) \dot{\varepsilon} + \frac{\eta_1 \eta_2 (E_1 + E_2)}{E_1 E_2} \ddot{\varepsilon}$
Burgers Material (Kelvin representation)		$\sigma + \left( \frac{\eta_1}{E_1} + \frac{\eta_2}{E_1} + \frac{\eta_2}{E_2} \right) \dot{\sigma} + \frac{\eta_1 \eta_2}{E_1 E_2} \ddot{\sigma} = \eta_2 \dot{\varepsilon} + \frac{\eta_1 \eta_2}{E_1} \ddot{\varepsilon}$

#### 4.4. Scope of Application Results

CIATIM-221 is widely used in bridge bearings. The lubricant must operate over a wide temperature range and retain its structure. Increasing the durability of structural elements is one of the urgent tasks of bridge building [73]. A large amount of research is related to numerical modeling and computer engineering (Section 4.2.). However, the dynamic characteristics of materials must be taken into account to analyze the behavior of the structure over time (Section 4.3.). Using the approaches described above will enable:

- Numerical experiments to be conducted on the operation of structural elements during the life cycle;
- Extension of the presented study to determine the rheological properties of polymeric materials [74];
- Consideration of the possibility of using a set of materials in structural elements at the decision-making stage [75,76];
- The reduction of material and time costs for field research, etc.

## 5. Conclusions

The main goal of the research is to conduct natural experiments and identify a mathematical model of the lubricant. The object of the study is the lubricant CIATIM-221, which is widely used in bridge structures with a working temperature range of  $-60$  °C to  $+60$  °C.

For the experimental study, the rotational viscometer Discovery HR2 was chosen. The experimental investigations were carried out in the temperature range of  $-40$  to  $+80$  °C. In the course of the work, a methodology for determining rheological characteristics based on oscillatory research was proposed. During the experiment, it was found that the lubricant is in a gel-like or elastic state over the entire temperature range.

The second stage of the research is aimed at identifying a mathematical model of the behavior of the lubricant. In the course of the work, it was assumed that the lubricant behaves like a Maxwell body. Two mathematical models of viscoelastic behavior were chosen: the Anand model and the Prony series. It was found that the mathematical model describes the behavior of the material well depending on the temperature. However, depending on the frequency of the sample's action, there are differences:

- At higher frequencies, the error is minimal;
- At low frequencies, there is a significant error.

Therefore, the lubricant does not behave like a Maxwell body at low frequencies. The presented model can only be applied at higher frequencies. For low frequencies, more complex models of viscoelastic behavior of the material are required.

**Author Contributions:** Conceptualization, A.A.K. and Y.O.N.; methodology, A.A.K.; software, A.A.K. and Y.O.N.; validation, A.A.K.; writing—original draft preparation, A.A.K. and Y.O.N.;

writing—review and editing, A.A.K. and Y.O.N.; visualization, A.A.K. and Y.O.N.; funding acquisition, A.A.K. All authors have read and agreed to the published version of the manuscript.

**Funding:** The study supported by a grant of Russian Science Foundation (project No. 22-29-01313).

**Data Availability Statement:** Not applicable.

**Conflicts of Interest:** The authors declare no conflict of interest.

## Nomenclature

$\varphi$	angular displacement of the rheometer;
$G^*$	complex shear modulus;
$\gamma$	shear strain;
$\tau_e$	tangential stress of an elastic element;
$\gamma_e$	shear strain of an elastic element;
$\tau_v$	tangential stress of a viscous element;
$\eta$	viscosity;
$\dot{\gamma}_v$	the rate of viscous shear strain;
$f$	functional;
$\tau_{\text{exp}}$	experimental tangential stress;
$\tau_{\text{num}}$	numerical tangential stress;
$\bar{x}$	vector of unknowns;
$G_\infty$	long shear modulus;
$G_0$	initial shear modulus;
$\alpha_i$	weight coefficients;
$\beta'_i$	reduced time;
$k$	number of relaxation times;
$A_{WLF}(T)$	temperature-time analogy shift function;
$T$	absolute temperature;
$C_1, C_2$	empirical material constants;
$T_r$	base temperature;
$A$	pre-exponential multiplier;
$U$	activation energy;
$R$	universal gas constant;
$\xi$	stress multiplier;
$S$	shear strain resistance;
$h_0$	material hardening constant;
$S^*$	saturation value of the hardening function;
$n$	sample saturation as a function of shear rate.

## References

1. Wen, C.; Meng, X.; Gu, J.; Xiao, L.; Jiang, S.; Bi, H. Starved lubrication analysis of angular contact ball bearing based on a multi-degree-of-freedom tribo-dynamic model. *Friction* **2023**, *11*, 1395–1418. [[CrossRef](#)]
2. Stahl, L.; Müller, M.; Ostermeyer, G.P. On the experimental characterization of the fluid volume influence on the friction between rough surfaces. *Friction* **2023**, *11*, 1334–1348. [[CrossRef](#)]
3. Jiang, S.; Liu, J.; Yang, Y.; Lin, Y.; Zhao, M. Experimental research and dynamics analysis of multi-link rigid–flexible coupling mechanism with multiple lubrication clearances. *Arch. Appl. Mech.* **2023**, *93*, 2749–2780. [[CrossRef](#)]
4. Sokolov, N.V.; Khadiev, M.B.; Fedotov, P.E.; Fedotov, E.M. Influence of the Lubricant’s Supply Temperature on the Operation of a Fluid Film Thrust Bearing. *Russ. Eng. Res.* **2023**, *43*, 264–271. [[CrossRef](#)]
5. Li, Y.; Shi, L.; Liu, Z.; Wang, X.; Qiao, X.; Zhang, Z.; Yan, S. Study on the lubrication state and pitting damage of spur gear using a 3D mixed EHL model with fractal surface roughness. *J. Mech. Sci. Technol.* **2022**, *36*, 5947–5957. [[CrossRef](#)]
6. Cao, W.; He, T.; Pu, W.; Xiao, K. Dynamics of lubricated spiral bevel gears under different contact paths. *Friction* **2022**, *10*, 247–267. [[CrossRef](#)]
7. Zhang, Y.; Shakil, A.; Humood, M.; Polycarpou, A.A. Finite element simulations of sliding contact of the head-disk interface in magnetic storage with lubricant effects. *Appl. Surf. Sci. Adv.* **2021**, *6*, 100155. [[CrossRef](#)]
8. Smith, E.H. On the Design and Lubrication of Water-Lubricated, Rubber, Cutlass Bearings Operating in the Soft EHL Regime. *Lubricants* **2020**, *8*, 75. [[CrossRef](#)]
9. Wang, P.; Qiu, J.; Gao, P.; Dong, R.; Han, Y.; Fan, M. The tribological behaviors and anti-corrosion performances of 5-phenyltetrazole ionic liquid additives for water lubricants. *Wear* **2023**, *516–517*, 204621. [[CrossRef](#)]

10. Sharma, S.C.; Singh, A. A study of double layer conical porous hybrid journal bearing operated with non-Newtonian lubricant. *Tribol. Int.* **2023**, *179*, 108183. [[CrossRef](#)]
11. Qiu, Y.L.; Zhou, C.G.; Ou, Y.; Feng, F.T. Theoretical and experimental analysis of the temperature rise of a ball screw. *Int. J. Adv. Manuf. Technol.* **2023**, *127*, 703–715. [[CrossRef](#)]
12. Li, Z.; Shen, H.; Liang, K.; Chen, X.; Zhu, Z. A numerical study on the effect of oil lubricant on the heat transfer and efficiency of a vapour compression refrigeration system. *Int. Commun. Heat Mass Transf.* **2022**, *134*, 106016. [[CrossRef](#)]
13. Torabi, A.; Alidousti, M.H. Numerical and experimental study of elastohydrodynamic grease lubrication of dimple textured surfaces. *Acta Mech.* **2023**, *234*, 2919–2931. [[CrossRef](#)]
14. Dang, R.K.; Goyal, D.; Chauhan, A.; Dhama, S.S. Numerical and Experimental Studies on Performance Enhancement of Journal Bearings Using Nanoparticles Based Lubricants. *Arch. Comput. Methods Eng.* **2021**, *28*, 3887–3915. [[CrossRef](#)]
15. Jadhav, S.; Thakre, G.D.; Sharma, S.C. Numerical modeling of elastohydrodynamic lubrication of line contact lubricated with micropolar fluid. *J. Braz. Soc. Mech. Sci. Eng.* **2018**, *40*, 326. [[CrossRef](#)]
16. Summer, F.; Bergmann, P.; Grün, F. On the Wear Behaviour of Bush Drive Chains: Part II—Performance Screening of Pin Materials and Lubricant Effects. *Lubricants* **2023**, *11*, 157. [[CrossRef](#)]
17. Bouchehit, B.; Bou-Said, B.; Tichy, J. Towards Ecological Alternatives in Bearing Lubrication. *Lubricants* **2021**, *9*, 62. [[CrossRef](#)]
18. Nosov, Y.O.; Kamenskikh, A.A. Influence Analysis of Lubricant Recesses on the Working Capacity of the Bridge Span Spherical Bearing. *Lubricants* **2022**, *10*, 283. [[CrossRef](#)]
19. Wu, P.; Chen, J.; Sojka, P.E.; Li, Y.; Cao, H. Experimental study of the lubricant-refrigerant flow in a rotary compressor. *Int. J. Refrig.* **2023**. [[CrossRef](#)]
20. Singh, N.; Sinha, S.K. Tribological and mechanical analysis of hybrid epoxy based polymer composites with different in situ liquid lubricants (silicone oil, PAO and SN150 base oil). *Wear* **2022**, *504–505*, 204404. [[CrossRef](#)]
21. Katsaros, K.P.; Nikolakopoulos, P.G. Performance Prediction Model for Hydrodynamically Lubricated Tilting Pad Thrust Bearings Operating under Incomplete Oil Film with the Combination of Numerical and Machine-Learning Techniques. *Lubricants* **2023**, *11*, 113. [[CrossRef](#)]
22. Tomanik, E.; Aubanel, L.; Bussas, M.; Delloro, F.; Lampke, T. Tribological Performance of a Composite Cold Spray for Coated Bores. *Lubricants* **2023**, *11*, 127. [[CrossRef](#)]
23. Qiang, H.; Gao, G.; Ye, S.; Cheng, L.; Wang, Q. Effect of Characteristic Parameters and Distribution of Friction Pair Surface Texture on Lubrication Properties. *Lubricants* **2023**, *11*, 139. [[CrossRef](#)]
24. Kodnyanko, V.; Shatokhin, S.; Kurzakov, A.; Pikalov, Y. Mathematical Modeling on Statics and Dynamics of Aerostatic Thrust Bearing with External Combined Throttling and Elastic Orifice Fluid Flow Regulation. *Lubricants* **2020**, *8*, 57. [[CrossRef](#)]
25. Orozco Lozano, W.; Fonseca-Vigoya, M.D.S.; Pabón-León, J. Study of the Kinematics and Dynamics of the Ring Pack of a Diesel Engine by Means of the Construction of CFD Model in Conjunction with Mathematical Models. *Lubricants* **2021**, *9*, 116. [[CrossRef](#)]
26. Yang, H.; Majeed, A.; Al-Khaled, K.; Abbas, T.; Naeem, M.; Khan, S.U.; Saeed, M. Significance of Melting Heat Transfer and Brownian Motion on Flow of Powell–Eyring Fluid Conveying Nano-Sized Particles with Improved Energy Systems. *Lubricants* **2023**, *11*, 32. [[CrossRef](#)]
27. Valigi, M.C.; Malvezzi, M.; Logozzo, S. A Numerical Procedure Based on Orowan’s Theory for Predicting the Behavior of the Cold Rolling Mill Process in Full Film Lubrication. *Lubricants* **2020**, *8*, 2. [[CrossRef](#)]
28. Poliakov, A.M.; Pakhaliuk, V.I. Predictive Estimates of Short-Term and Long-Term Results for Regenerative Rehabilitation of Local Articular Cartilage Defects in Synovial Joints. *Lubricants* **2023**, *11*, 116. [[CrossRef](#)]
29. Slabka, I.; Henniger, S.; Küçükaya, D.; Dawoud, M.; Schwarze, H. Influence of Rheological Properties of Lithium Greases on Operating Behavior in Oscillating Rolling Bearings at a Small Swivel Angle. *Lubricants* **2022**, *10*, 163. [[CrossRef](#)]
30. Farré-Lladós, J.; Westerberg, L.G.; Casals-Terré, J.; Leckner, J.; Westbroek, R. On the Flow Dynamics of Polymer Greases. *Lubricants* **2022**, *10*, 66. [[CrossRef](#)]
31. Conrad, A.; Hodapp, A.; Hochstein, B.; Willenbacher, N.; Jacob, K.-H. Low-Temperature Rheology and Thermoanalytical Investigation of Lubricating Greases: Influence of Thickener Type and Concentration on Melting, Crystallization and Glass Transition. *Lubricants* **2022**, *10*, 1. [[CrossRef](#)]
32. Li, X.K.; Luo, Y.; Qi, Y.; Zhang, R. On non-Newtonian lubrication with the upper convected Maxwell model. *Appl. Math. Model.* **2011**, *35*, 2309–2323. [[CrossRef](#)]
33. Madsen, E.; Rosenlund, O.S.; Brandt, D.; Zhang, X. Adaptive feedforward control of a collaborative industrial robot manipulator using a novel extension of the Generalized Maxwell-Slip friction model. *Mech. Mach. Theory* **2021**, *155*, 104109. [[CrossRef](#)]
34. Suarez-Afanador, C.A.; Cornaggia, R.; Lahellec, N.; Maurel-Pantel, A.; Boussaa, D.; Moulinec, H.; Bordas, S.P.A. Effective thermo-viscoelastic behavior of short fiber reinforced thermo-rheologically simple polymers: An application to high temperature fiber reinforced additive manufacturing. *Eur. J. Mech. A/Solids* **2022**, *96*, 104701. [[CrossRef](#)]
35. Sun, Y.; Huang, B.; Chen, J.; Jia, X.; Ding, Y. Characterizing rheological behavior of asphalt binder over a complete range of pavement service loading frequency and temperature. *Constr. Build. Mater.* **2016**, *123*, 661–672. [[CrossRef](#)]
36. Zhang, X.; Gu, X.; Lv, J.; Zou, X. 3D numerical model to investigate the rheological properties of basalt fiber reinforced asphalt-like materials. *Constr. Build. Mater.* **2017**, *138*, 185–194. [[CrossRef](#)]
37. Lesnikova, Y.I.; Trufanov, A.N.; Kamenskikh, A.A. Analysis of the Polymer Two-Layer Protective Coating Impact on Panda-Type Optical Fiber under Bending. *Polymers* **2022**, *14*, 3840. [[CrossRef](#)]

38. Sakhabutdinova, L.R.; Smetannikov, O.Y.; Il'inykh, G.V. Numerical Simulation of the Process Manufacture of Large-Scale Composite Shell Taking Into Account Thermo Viscoelastic. *Tomsk. State Univ. J. Math. Mech.* **2022**, *76*, 165–181. [[CrossRef](#)]
39. Nuwayer, H.M.; Newaz, G.M. Flexural Creep Behavior of Adhesively Bonded Metal and Composite Laminates. *Int. J. Adhes. Adhes.* **2018**, *84*, 220–226. [[CrossRef](#)]
40. Anand, L. Constitutive Equations for Hot-Working of Metals. *Int. J. Plast.* **1985**, *3*, 213–231. [[CrossRef](#)]
41. Puchi-Cabrera, E.S.; Guérin, J.D.; Barbera-Sosa, J.G.; Dubar, M.; Dubar, L. Plausible Extension of Anand's Model to Metals Exhibiting Dynamic Recrystallization and its Experimental Validation. *Int. J. Plast.* **2018**, *108*, 70–87. [[CrossRef](#)]
42. Liu, E.; Bhogaraju, S.K.; Wunderle, B.; Elger, G. Investigation of stress relaxation in SAC305 with micro-Raman spectroscopy. *Microelectron. Reliab.* **2022**, *138*, 114664. [[CrossRef](#)]
43. Liang, Z.; Yonghuan, G.; Lei, S.; Chengwen, H. Reliability of SnAgCuFe Solder Joints in WLCSP30 Device. *Rare Met. Mater. Eng.* **2016**, *45*, 2823–2826. [[CrossRef](#)]
44. Larson, R.G.; Wei, Y. A Review of Thixotropy and its Rheological Modeling. *J. Rheol.* **2019**, *63*, 477–501. [[CrossRef](#)]
45. Hu, Y.; Wang, X.; Gao, Y.; Xu, J.; Ding, Y. Numerical Simulation of Effect of Glass Lubricant on Hot Extrusion of Inconel 625 Alloy Tubes. *Procedia Manuf.* **2019**, *37*, 119–126. [[CrossRef](#)]
46. Wolak, A.; Zając, G.; Słowik, T. Measuring Kinematic Viscosity of Engine Oils: A Comparison of Data Obtained from Four Different Devices. *Sensors* **2021**, *21*, 2530. [[CrossRef](#)]
47. Cerpa-Naranjo, A.; Pérez-Piñeiro, J.; Navajas-Chocarro, P.; Arce, M.P.; Lado-Touriño, I.; Barrios-Bermúdez, N.; Moreno, R.; Rojas-Cervantes, M.L. Rheological Properties of Different Graphene Nanomaterials in Biological Media. *Materials* **2022**, *15*, 3593. [[CrossRef](#)]
48. Kaushik, S.; Sonebi, M.; Amato, G.; Das, U.K.; Perrot, A. Optimisation of Mix Proportion of 3D Printable Mortar Based on Rheological Properties and Material Strength Using Factorial Design of Experiment. *Materials* **2023**, *16*, 1748. [[CrossRef](#)]
49. Xue, X.; Gao, J.; Wang, J.; Chen, Y. Evaluation of High-Temperature and Low-Temperature Performances of Lignin–Waste Engine Oil Modified Asphalt Binder and Its Mixture. *Materials* **2022**, *15*, 52. [[CrossRef](#)]
50. Peng, Y.; Via, B. The Effect of Cellulose Nanocrystal Suspension Treatment on Suspension Viscosity and Casted Film Property. *Polymers* **2021**, *13*, 2168. [[CrossRef](#)]
51. Quan, L.; Kalyon, D.M. Parallel-Disk Viscometry of a Viscoplastic Hydrogel: Yield Stress and Other Parameters of Shear Viscosity and Wall Slip. *Gels* **2022**, *8*, 230. [[CrossRef](#)]
52. Kozdrach, R. The Innovative Research Methodology of Tribological and Rheological Properties of Lubricating Grease. *Tribol. Ind.* **2021**, *43*, 117–130. [[CrossRef](#)]
53. Trufanova, N.M.; Ershov, S.V. Comparative Analysis of Heat and Mass Transfer Processes in the Extruder Dosing Zone with the Use Different Spatial Mathematical Model and Rheological Law. *J. Appl. Mech. Tech. Phys.* **2017**, *2*, 153–163. [[CrossRef](#)]
54. Davydova, V.A.; Shcherbinin, A.G.; Naumiv, M.D.; Ershov, S.V. A Numerical Study on Induction-Resistive Electric-Heating Processes of Pipelines. *Russ. Electr. Eng.* **2021**, *11*, 668–671. [[CrossRef](#)]
55. Schramm, G. *A Practical Approach to Rheology and Rheometry*; Gebrueder HAAKE GmbH: Karlsruhe, Germany, 1994; 290p.
56. Barnes, A.H. *A Handbook of Elementary Rheology*; University of Wales, Institute of Non-Newtonian Fluid Mechanics: Cardiff, Wales, 2000; 200p.
57. Zhai, M.; Zhou, K.; Sun, Z.; Xiong, Z.; Du, Q.; Zhang, Y.; Shi, L.; Hou, J. Rheological Characterization and Shear Viscosity Prediction of Heavy Oil-in-Water Emulsions. *J. Mol. Liq.* **2023**, *381*, 121782. [[CrossRef](#)]
58. Song, Y.; Won, C.; Kang, S.; Lee, H.; Park, S.; Park, S.H.; Yoon, J. Characterization of Gglass Viscosity with Parallel Plate and Rotational Viscometry. *J. Non-Cryst. Solids* **2018**, *486*, 27–35. [[CrossRef](#)]
59. Cherecheș, E.I.; Ibanescu, C.; Danu, M.; Minea, A.A. Studies on Rheological Properties and Isobaric Heat Capacity of ZnO-[C4mim][BF4] Nanoparticle Enhanced Ionic Liquid. *J. Mol. Liq.* **2023**, *380*, 121759. [[CrossRef](#)]
60. Romanova, Y.N.; Koroleva, M.Y.; Musina, N.S.; Maryutina, T.A. Rheology of Gel-Containing Water-in-Crude Oil Emulsions. *Geoenergy Sci. Eng.* **2023**, *226*, 211757. [[CrossRef](#)]
61. Adamov, A.A.; Kamenskikh, A.A.; Pankova, A.P.; Strukova, V.I. Comparative Analysis of the Work of Bridge Spherical Bearing at Different Antifriction Layer Locations. *Lubricants* **2022**, *10*, 207. [[CrossRef](#)]
62. Kim, J.-H.; Kim, W.S.; Yoo, Y. Friction Properties of Solid Lubricants with Different Multiwalled Carbon Nanotube Contents. *Materials* **2022**, *15*, 4054. [[CrossRef](#)]
63. Adamov, A.A.; Kamenskikh, A.A.; Pankova, A.P. Influence Analysis of the Antifriction Layer Materials and Thickness on the Contact Interaction of Spherical Bearings Elements. *Lubricants* **2022**, *10*, 30. [[CrossRef](#)]
64. Chong, W.W.F.; Hamdan, S.H.; Wong, K.J.; Yusup, S. Modelling Transitions in Regimes of Lubrication for Rough Surface Contact. *Lubricants* **2019**, *7*, 77. [[CrossRef](#)]
65. Mukutadze, M.A.; Lagunova, E.O. Mathematical Model of Flow of Lubricant and Molten Coating with Micropolar Rheological Properties in Running Clearance of Journal Bearing with Non-circular Bearing Surface Profile, Considering Pressure Dependence of Viscosity. In *Proceedings of the 8th International Conference on Industrial Engineering, Belgrade, Serbia, 29–30 September 2022*; ICIE, Lecture Notes in Mechanical Engineering; Springer: Cham, Switzerland, 2022; pp. 587–597. [[CrossRef](#)]
66. Jadhao, V.; Robbins, M.O. Rheological Properties of Liquids Under Conditions of Elastohydrodynamic Lubrication. *Tribol. Lett.* **2019**, *67*, 66. [[CrossRef](#)]

67. Gamani, S.S.; Dini, D.; Biancofiore, L. The Effect of Fluid Viscoelasticity in Lubricated Contacts in the Presence of Cavitation. *Tribol. Int.* **2021**, *160*, 107011. [[CrossRef](#)]
68. Ivins, E.R.; Caron, L.; Adhikari, S.; Larour, E. Notes on a Compressible Extended Burgers Model of Rheology. *Geophys. J. Int.* **2022**, *228*, 1975–1991. [[CrossRef](#)]
69. Kvarda, D.; Skurka, S.; Galas, R.; Omasta, M.; Shi, L.; Ding, H.; Wang, W.; Krupka, I.; Hartl, M. The Effect of Top of Rail Lubricant Composition on Adhesion and Rheological Behaviour. *Eng. Sci. Technol. Int. J.* **2022**, *35*, 101100. [[CrossRef](#)]
70. Mujumdar, A.; Beris, A.N.; Metzner, A.B. Transient Phenomena in Thixotropic Systems. *J. Non-Newton. Fluid Mech.* **2002**, *102*, 157–178. [[CrossRef](#)]
71. Mendes, P.R.; Thompson, R.L. A Critical Overview of Elasto-Viscoplastic Thixotropic Modeling. *J. Non-Newton. Fluid Mech.* **2012**, *187–188*, 8–15. [[CrossRef](#)]
72. Radhakrishnan, R.; Divous, T.; Manneville, S.; Fielding, S.M. Understanding Rheological Hysteresis in Soft Glassy Materials. *Soft Matter* **2017**, *9*, 1834–1852. [[CrossRef](#)]
73. Niemierko, A. Modern Bridge Bearings and Expansion Joints for Road Bridges. *Trans. Res. Procedia* **2016**, *14*, 4040–4049. [[CrossRef](#)]
74. Yi, X.; Du, S.; Zhang, L. *Composite Materials Engineering, Volume 1: Fundamentals of Composite Materials*; Springer: Singapore, 2018. [[CrossRef](#)]
75. Adamov, A.A.; Kamenskih, A.A.; Pankova, A.P. Numerical analysis of the spherical bearing geometric configuration with antifricition layer made of different materials. *PNRPU Mech. Bull.* **2020**, *4*, 15–26. [[CrossRef](#)]
76. Ono, K. Structural materials: Metallurgy of bridges. In *Metallurgical Design and Industry*; Springer: Cham, Switzerland, 2018; pp. 193–269. [[CrossRef](#)]

**Disclaimer/Publisher’s Note:** The statements, opinions and data contained in all publications are solely those of the individual author(s) and contributor(s) and not of MDPI and/or the editor(s). MDPI and/or the editor(s) disclaim responsibility for any injury to people or property resulting from any ideas, methods, instructions or products referred to in the content.